Fluorescence Quenching of Dye Molecules near Gold Nanoparticles: Radiative and Nonradiative Effects

E. Dulkeith, A. C. Morteani, T. Niedereichholz, T. A. Klar, and J. Feldmann
Photonics and Optoelectronics Group, Physics Department and CeNS, University of Munich, 80799 Munich, Germany

S. A. Levi, F. C. J. M. van Veggel, and D. N. Reinhoudt
Laboratories for Supramolecular Chemistry and Technology, University of Twente, 7500 AE Enschede, The Netherlands

M. Möller
Abteilung Organische Chemie III/Macromolekulare Chemie-OC III, Universität Ulm, 89069 Ulm, Germany

D. I. Gittins
Max Planck Institute of Colloids and Interfaces, 14424 Potsdam, Germany
(Received 28 February 2002; published 24 October 2002)

The radiative and nonradiative decay rates of lissamine dye molecules, chemically attached to differently sized gold nanoparticles, are investigated by means of time-resolved fluorescence experiments. A pronounced fluorescence quenching is observed already for the smallest nanoparticles of 1 nm radius. The quenching is caused not only by an increased nonradiative rate but, equally important, by a drastic decrease in the dye's radiative rate. Assuming resonant energy transfer to be responsible for the nonradiative decay channel, we compare our experimental findings with theoretical results derived from the Gersten-Nitzan model.

DOI: 10.1103/PhysRevLett.89.203002 PACS numbers: 33.50.-j, 81.07.Pr

Resonant energy transfer (RET) systems consisting of organic dye molecules and noble metal nanoparticles have recently gained considerable interest in biophotonics [1–4] as well as in materials science [5,6]. Closely related are donor-acceptor pairs of organic dye molecules forming Förster resonant energy transfer (FRET) systems. They have been theoretically modeled [7] and applied in biophysics extensively during the past decade (see, e.g., [8]). Yet these classical purely dye-based systems show disadvantages regarding quenching efficiency [4] and photostability [9].

If the donor molecule is placed in the vicinity of a metal surface instead of an organic acceptor, not only resonant energy transfer takes place but also the radiative lifetime of the donor molecule changes. For metal films this has been investigated extensively [10–13]. Much less is known about donor molecules in the vicinity of metal nanoparticles. Theoretical treatments of the molecule-nanoparticle problem [14–17] predict energy transfer rates and radiative decay rates that deviate substantially from what has been found for dye molecules in front of a metal film. Both radiative and nonradiative rates are expected to depend critically on size and shape of the nanoparticle, the distance between the dye molecule and the nanoparticle, the orientation of the molecular dipole with respect to the dye-nanoparticle axis, and the overlap of the molecule's emission with the nanoparticle's absorption spectrum. Recent experimental investigations deal with metal island films or rough surfaces only (see [18,19] and references in [20]), where the above mentioned parameters are undefined.

Here we report results of time-resolved fluorescence experiments on a donor-acceptor system composed of lissamine molecules (donor) chemically attached to a gold nanoparticle (acceptor). The distance between the lissamine molecule and the surface of the nanoparticle is kept constant at 1 nm, whereas the nanoparticle radius is varied between 1 and 30 nm. We find time constants for the energy transfer on a picosecond time scale which turn out to decrease with increasing nanoparticle size. In addition, the dye's radiative rate is reduced by more than an order of magnitude. Both effects are responsible for the drastic quenching of the fluorescence yield as predicted by the so-called Gersten-Nitzan model [14].

Figure 1 sketches the RET system under investigation. Lissamine dye molecules are attached to gold nanoparticles of radius r (dispersion $<15\%$) via a thioether group [21]. For all particle radii the concentrations of lissamine were chosen in order to achieve 50% coverage of the nanoparticles. This value can be estimated by assuming that one dye molecule covers approximately 1 nm^2 of surface area. All investigations are done in aqueous solution in order to match biological conditions.

The frequency-doubled output (400 nm) of a Kerr-lens mode-locked titanium-sapphire laser (120 fs, 76 MHz) is used as the optical excitation source. The samples' emission is dispersed either spectrally using a grating spectrometer together with an intensified CCD camera (Picostar HR12, LaVision) or temporally by using a streak camera with a temporal resolution of 2 ps (C 5680, Hamamatsu). Appropriate spectral filters are used to block any stray light from the excitation beam. All

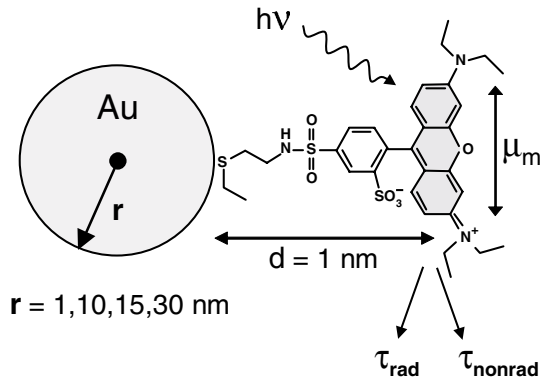

FIG. 1. Lissamine dye molecules are attached to gold nanoparticles via a thioether group. The radii of the nanoparticles vary between 1 and 30 nm. The optical dipole moment μ_m of the π-conjugated part of the molecule is oriented perpendicular to the dye-particle axis and situated approximately 1 nm from the particle's surface.

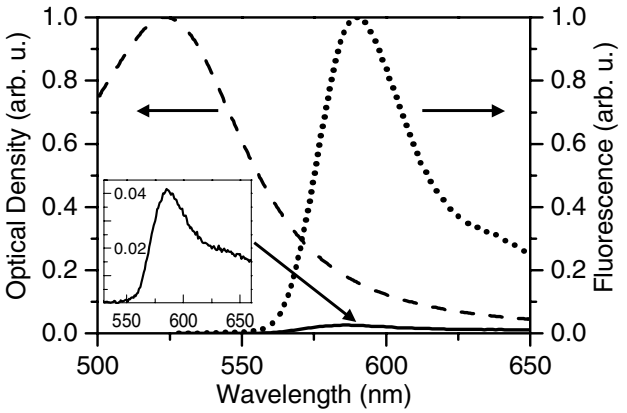

FIG. 2. Optical density spectrum of a gold nanoparticle solution with $r = 15$ nm (dashed curve), fluorescence spectra of a 0.37 μM aqueous solution of lissamine dye molecules before (dotted curve) and after attaching to gold nanoparticles with $r = 15$ nm (solid curve and inset). A drastic fluorescence quenching is observed.

experiments are performed at room temperature. It is important to note that the excitation wavelength of 400 nm does not coincide with the plasmon resonance peaks. Therefore, the change in molecular absorption mediated by the electrical near field due to a particle plasmon resonance is weak. Assuming that absorption and emission probabilities are proportional, we can use the Gersten-Nitzan theory to calculate the decrease of absorption cross section at 400 nm (e.g., 35% for a nanoparticle radius of 15 nm).

Figure 2 displays optical spectra of the two isolated subunits, gold nanoparticles and unbound lissamine molecules, as well as the quenched fluorescence spectrum of the composite system. The dashed curve shows the optical density spectrum of a solution of gold nanoparticles of $r = 15$ nm. The surface plasmon peak at a wavelength of 520 nm is readily observed [22]. The dotted line represents the fluorescence spectrum of a 0.37 μM aqueous solution of unbound lissamine dye molecules. This spectrum is already corrected for the absorption of excitation light and reabsorption of molecular fluorescence light due to the presence of the gold nanoparticles as well as the near field effects on the absorption cross section (called "trivial effects" in the following). The solid curve and the inset of Fig. 2 show the remaining fluorescence when a 0.37 μM dye solution is mixed with $r = 15$ nm gold nanoparticles forming hybrid systems as sketched in Fig. 1. The fluorescence is quenched by at least 95%. As will be discussed later, the majority of these remaining 5% is due to fluorescence from unbound dye molecules leading to a quenching efficiency of more than 99%.

Before dealing with the time-resolved optical emission spectra of the hybrid dye-nanoparticle systems, we first present the results of the two isolated solutions. The inset of Fig. 3(a) shows the time-resolved optical emission curve of a 0.25 nM solution of $r = 15$ nm gold nanoparticles. A pulsed emission at $t = 0$ is observed, the temporal evolution of which cannot be resolved by the streak camera. From a spectral analysis we conclude that this fast emission signal is due to a continuum Raman emission background [23].

The time-resolved fluorescence spectrum of the 0.37 μM aqueous solution of pure lissamine molecules is shown in a semilogarithmic plot in Fig. 3(b) (again corrected for trivial effects). From the monoexponential decay a time constant of $\tau_{fluo} = R_{fluo}^{-1} = 1.54$ ns is derived for the total fluorescence lifetime. Together with the known quantum efficiency η of 33% [24] for such unbound lissamine molecules in aqueous solution a radiative decay rate of $R_{rad} = 0.21 \times 10^9\ s^{-1}$ is obtained. In the following, these values are named $R_{fluo}(r = 0)$, $R_{rad}(r = 0)$, $R_{nonrad}(r = 0)$, and $\eta(r = 0)$.

The experimentally found emission transient of a hybrid lissamine/Au-nanoparticle solution is shown in Fig. 3(a). The lissamine and Au-nanoparticle, the nanoparticle radius, as well as the experimental conditions are exactly the same as for the isolated solutions. Three components can be identified in the decay dynamics. As expected, the presence of gold nanoparticles again leads to the fast emission signal at $t = 0$ with the same peak intensity as in the inset. For time values larger than 300 ps the emission decay kinetics resembles the fluorescence decay known for unbound lissamine dye molecules from Fig. 3(b). This can be seen by comparing the long-living emission with the solid line drawn in Fig. 3(a), which represents a monoexponential decay function with a time constant $\tau_{fluo} = 1.54$ ns taken from the fluorescence decay in Fig. 3(b). Accordingly, we attribute this signal contribution to unbound lissamine dye molecules. Because of the thermodynamic equilibrium condition between bound and unbound lissamine molecules, it is impossible to eliminate completely the excess of dye by cleaning or dialysis procedures. Obviously, the identification of the short- and long-living emission components allows one to subtract the gold nanoparticle emission

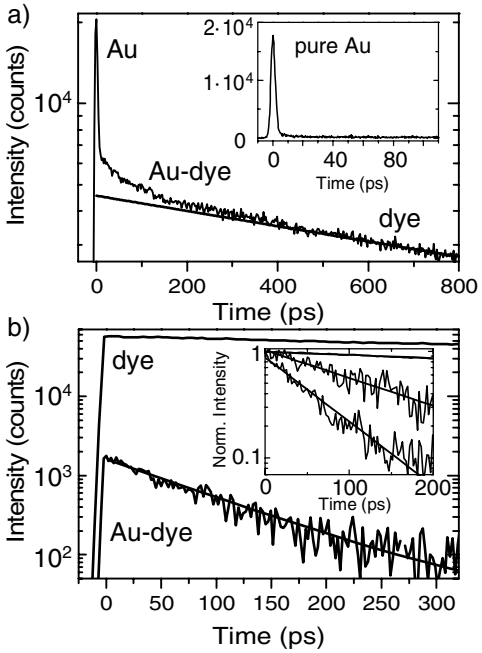

FIG. 3. Time-resolved optical emission spectra: (a) solution containing the composite gold/dye system (Fig. 1, $r = 15$ nm) and pure gold nanoparticle solution ($r = 15$ nm, inset); (b) comparison of pure dye and composite gold/dye ($r = 15$ nm) after removal of background signals (see text for details). Inset: free dye and composite Au/dye with $r = 1$ and 30 nm for decay times of 1.54 ns, 169 ps, and 72 ps, respectively.

curve and the fluorescence curve of the unbound lissamine molecules as given by the solid line in Fig. 3(a) from the emission curve of the hybrid solution. Applying these corrections, only the intermediate fluorescence decay signal from the lissamine dye molecules bound to gold nanoparticles is left over.

This decay signal is shown on a logarithmic scale in Fig. 3(b). The inset of Fig. 3(b) shows the fluorescence transients of the hybrid system for nanoparticle radii of $r = 1$ and 30 nm. All Au-dye fluorescence transients turn out to decay monoexponentially, and hence heterogeneity of the two-particle systems cannot play a dominant role. The fluorescence lifetimes $R_{\mathrm{fluo}}(r)^{-1}$ are 169, 99, and 72 ps in the case of $r = 1$, 15, and 30 nm nanoparticles, respectively. Obviously, the fluorescence lifetime decreases monotonically with increasing nanoparticle radius. Compared to the free dye's lifetime of 1.54 ns a substantial shortening has occurred. In addition, we observe a pronounced quenching of the Au-dye fluorescence transients already at $t = 0$. As discussed in the following, this is a direct consequence of a drastically reduced radiative decay rate.

To obtain more quantitative information we write the radius dependent fluorescence decay rate $R_{\mathrm{fluo}}(r)$ as

$$R_{\mathrm{fluo}}(r) = R_{\mathrm{nonrad}}(r) + R_{\mathrm{rad}}(r) \qquad (1)$$

and the fluorescence quantum efficiency $\eta(r)$ as

$$\eta(r) = R_{\mathrm{rad}}(r)/R_{\mathrm{fluo}}(r) = g\int_0^\infty I_{\mathrm{fl}}(r, t=0)e^{-tR_{\mathrm{fluo}}(r)}dt = gI_{\mathrm{fl}}(r, t=0)/R_{\mathrm{fluo}}(r). \qquad (2)$$

$I_{\mathrm{fl}}(r, t)$ is the measured fluorescence transient [as shown in Fig. 3(b)], and g is a collection efficiency factor taking care of emitted but not detected fluorescence photons in our experiment. Now, g can be determined from Eq. (2) for $r = 0$, since $\eta(r = 0)$, $I_{\mathrm{fl}}(r = 0, t = 0)$, and $R_{\mathrm{fluo}}(r = 0)$ are experimentally determined values. From Eq. (2) follows the simple relation $R_{\mathrm{rad}}(r) = gI_{\mathrm{fl}}(r, t = 0)$. In other words, the intensities of the Au-dye fluorescence transients at $t = 0$ are a direct measure of the radiative molecular decay rates [25]. Once the radiative decay rates $R_{\mathrm{rad}}(r)$ are known, we can deduce the nonradiative rates $R_{\mathrm{nonrad}}(r)$ from Eq. (1) using the experimentally determined fluorescence decay rates $R_{\mathrm{fluo}}(r)$ [Fig. 3(b)].

In Figs. 4(a) and 4(b) the experimentally determined radiative and nonradiative rates, $R_{\mathrm{rad}}(r)$ and $R_{\mathrm{nonrad}}(r)$, are plotted versus the radius of the gold nanoparticles (error bars smaller than the size of data points). The radiative rate R_{rad} of lissamine dye molecules drops by more than an order of magnitude, whereas their nonradiative rate $R_{\mathrm{nonrad}}(r)$ increases by more than an order of magnitude when attached to gold nanoparticles. We can conclude that both effects are responsible for the observed drastic fluorescence quenching in the vicinity of gold nanoparticles.

For lissamine molecules attached to the smallest $r = 1$ nm nanoparticles, the 51-times longer radiative lifetime and the 14-times shorter nonradiative lifetime lead to a reduction of the fluorescence quantum yield from 33% down to 0.07%. This corresponds to a quenching efficiency of 99.8% (for these $r = 1$ nm nanoparticles mainly induced by a reduction of the radiative rate). The fact that already the smallest nanoparticles of 1 nm

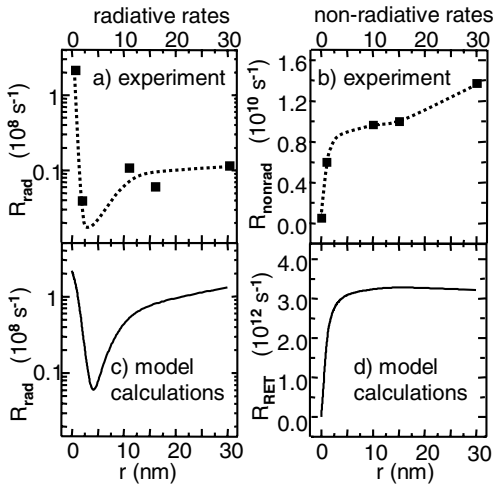

FIG. 4. Radiative and nonradiative rates as a function of particle radius; $r = 0$ indicates rates of the unbound dye. (a),(b) Experimentally determined radiative and nonradiative rates; lines are a guide to the eye. (c),(d) Calculated radiative and energy transfer rates based on the GN model [14].

radius induce such a pronounced quenching is an important finding. This allows gold nanoparticles to be used as acceptors in biophysical FRET experiments in vitro as well as in vivo [4]. Both applications require metal nanoparticles of minimum diameter to ensure that the system to be monitored is not mechanically disturbed.

We now compare our results with calculations based on the static model introduced by Gersten and Nitzan (GN). In particular, we use equations B.42′, B.43′, and B.45′ from the mathematical appendix of Ref. [14], however, with the refractive index of water instead of air and calculated at an emission wavelength of 595 nm. The dielectric function of gold is used as published in [26]. For dye-nanoparticle distances of 1 nm a static model should be accurate enough, and hence an electrodynamical treatment is not necessary [27]. Within the GN model the radiative rate R_{rad} is derived by assuming Hertzian dipole emitters. Here the dipole for the entire system is considered, taking into account the intrinsic molecular dipole, the molecular dipole induced by the dipole field of the adjacent nanoparticle, and the dipole of the nanoparticle driven by the dipole field of the molecule. The resonant energy transfer of the molecular excitation is treated by calculating the absorption of the molecular dipole field at the position of the metal nanoparticle.

For the present case of lissamine molecules attached to gold nanoparticles as depicted in Fig. 1 we have calculated the radiative rate R_{rad} and the transfer rate R_{RET} as a function of nanoparticle radius r, assuming the molecular dipole moment to be oriented parallel to the particle surface. The results are shown in Figs. 4(c) and 4(d). The radiative rate R_{rad} exhibits a pronounced minimum around $r = 4$ nm. This drastically decreased emission rate is in qualitative agreement with the experimental findings of Fig. 4(a) and is a consequence of a phase shift between the molecular and the metal dipole leading to a destructive interference effect. This situation can be compared with two adjacent antennas broadcasting inefficiently when out of phase. The phase shift is caused by the complex nature of the metal dielectric. The weak oscillatory behavior of R_{rad} versus r, present in the experimental findings but absent in the GN theory may be explained by a full electrodynamic theory [28].

Concerning shape, the size dependence of R_{RET} as seen in Fig. 4(d) closely follows the experimentally determined size dependence of R_{nonrad} [compared to Fig. 4(b)]. However, the calculated absolute values for R_{RET} are 2 orders of magnitude larger than the experimentally determined nonradiative rates R_{nonrad}. We attribute this discrepancy to the fact that the GN model does not take into account nonlocal effects which can easily reduce the transfer rate R_{RET} by 2 orders of magnitude if the molecule-nanoparticle distance is less than 5 nm [17]. Additionally, the approximation of the molecule as a point dipole may be too crude [29]. Further reasons for deviation from theory may be that the molecules are not exactly parallel to the particle's surface and the calculation is carried out at one single frequency ω instead of considering the spectral overlap integral as done in Förster theory. Electron transfer may give rise to another nonradiative decay process [30]; however, this would further increase the deviation of experimental values from theoretical ones.

We thank C. Sönnichsen and A. Nitzan for helpful discussions. This work has been supported by the Deutsche Forschungsgemeinschaft (DFG) through the SFB 486 and the Gottfried-Wilhelm-Leibniz Preis.

[1] R. D. Powell *et al.*, J. Histochem. Cytochem. **45**, 947 (1997).
[2] R. D. Powell, C. M. R. Halsey, and J. F. Hainfeld, Microsc. Res. Tech. **42**, 2 (1998).
[3] G. Peleg *et al.*, Proc. Natl. Acad. Sci. U.S.A. **96**, 6700 (1999).
[4] B. Dubertret, M. Calame, and A. J. Libchaber, Nature Biotech. **19**, 365 (2001).
[5] H. Imahori and S. Fukuzumi, Adv. Mater. **13**, 1197 (2001).
[6] H. Imahori *et al.*, J. Am. Chem. Soc. **123**, 335 (2001).
[7] T. Förster, Ann. Phys. **2**, 55 (1948).
[8] J. R. Lakowicz, *Principles of Fluorescence Spectroscopy* (Kluwer Academic, New York, 1999).
[9] S. Weiss, Science **283**, 1676 (1999).
[10] K. H. Drexhage *et al.*, Ber. Bunsen-Ges. Phys. Chem. **20**, 1179 (1966).
[11] R. R. Chance, A. Prock, and R. Silbey, in *Advances in Chemical Physics*, edited by I. Prigogine and S. R. Rice (Wiley, New York, 1978), p. 1.
[12] H. Imahori *et al.*, J. Phys. Chem. B **104**, 1253 (2000).
[13] P. Andrew and W. L. Barnes, Science **290**, 785 (2000).
[14] J. Gersten and A. Nitzan, J. Chem. Phys. **75**, 1139 (1981).
[15] R. Ruppin, J. Chem. Phys. **76**, 1681 (1982).
[16] H. Chew, J. Chem. Phys. **87**, 1355 (1987).
[17] P. T. Leung, Phys. Rev. B **42**, 7622 (1990).
[18] A. Leitner *et al.*, Appl. Phys. B **36**, 105 (1985).
[19] J. R. Lakowicz *et al.*, Anal. Biochem. **301**, 261 (2002).
[20] P. T. Leung and T. F. George, J. Chim. Phys. Phys.-Chim. Biol. **92**, 226 (1995).
[21] The sulfide was synthesized by reaction of 2-(ethylthio)-ethylamine with lissamine monosulfonyl chloride. For details on a similar compound see S. A. Levi *et al.*, Chem. Eur. J. **8**, 3808 (2002).
[22] U. Kreibig and M. Vollmer, *Optical Properties of Metal Clusters* (Springer-Verlag, Berlin, 1995).
[23] S. Nie and S. R. Emory, Science **275**, 1102 (1997).
[24] S. N. Smith and R. P. Steer, J. Photochem. Photobiol. A **139**, 151 (2001).
[25] F. R. Aussenegg *et al.*, Surf. Sci. **189**, 935 (1987).
[26] P. B. Johnson and R.W. Christy, Phys. Rev. B **6**, 4370 (1972).
[27] P. T. Leung and T. F. George, J. Chem. Phys. **87**, 6722 (1987).
[28] P. T. Leung, Y. S. Kim, and T. F. George, J. Phys. Chem. **92**, 6206 (1988).
[29] T. Maniv and H. Metiu, J. Chem. Phys. **72**, 1996 (1980).
[30] B. I. Ipe *et al.*, J. Phys. Chem. B **106**, 18 (2002).